# Influence of magnetic domain landscape on the flux dynamics in superconductor/ferromagnet bilayers

Z. Adamus and Marta Z. Cieplak
*Institute of Physics, Polish Academy of Sciences, 02 668 Warsaw, Poland*

M. Kończykowski
*Laboratoire des Solides Irradies, École Polytechnique, 91128 Palaiseau, France*

L. Y. Zhu and C. L. Chien
*Department of Physics and Astronomy, The Johns Hopkins University, Baltimore, Maryland 21218, USA*
(Received 13 January 2014; revised manuscript received 15 December 2015; published 8 February 2016)

We use a line of miniature Hall sensors to study the influence of the magnetic domain distribution on the flux dynamics in superconductor/ferromagnet bilayers. Two bilayers are built of a ferromagnetic Co/Pt multilayer with perpendicular magnetic anisotropy and a superconducting Nb layer, with the insulating layer in-between to avoid proximity effect. The magnetic domain patterns of various geometries are reversibly predefined in the Co/Pt multilayers using the appropriate magnetization procedure. The Pt thickness is different in the two bilayers, resulting in different width and length of the domains, which profoundly affects vortex dynamics. We show that narrow short domains lead to strong confinement of vortices at the sample edge, while narrow elongated domains of uniform width induce smaller confinement and easy vortex entry. Large enhancement of flux pinning and critical current density, by a factor of more than 7, is observed in the last case, while the former results in smaller enhancement. When domains are wide, the disorder in the domain widths becomes beneficial for larger enhancement of pinning, while more uniform distribution of domain widths results in a precipitous drop of the enhancement. The analysis of these results suggests that with increasing domain width, a transition occurs from vortex chains pinned by narrow domains to disordered triangular vortex lattice pinned by a maze of multiply interconnected magnetic domains.

DOI: 10.1103/PhysRevB.93.054509

## I. INTRODUCTION

The properties of type II superconductors in the mixed state depend on the dynamics of vortices, which in turn is strongly influenced by vortex pinning. The ability to modify pinning is important, both for the application of superconductivity and for the understanding of vortex matter, which itself is a model for systems of strongly interacting particles. One of the methods to modify vortex pinning may be realized in superconductor(S)/ferromagnet(F) bilayers (SFB), hybrid structures with thin S and F layers placed in close proximity [1–6]. If a magnetic texture exists in the F layer, the Cooper pairs interact with the magnetic fields emanating from the texture via the long-range electromagnetic interaction. This interaction modifies the superconducting phase transition line [3,7–12], and provides pinning potential for the vortices [1,6,13–21]. This last effect, called magnetic pinning, the focus of this work, may be most conveniently studied in SFBs with thin insulating layer inserted between the S and the F layer, thus cutting off short-range proximity effect [1,6].

The magnetic pinning has been extensively studied in the past, mostly in SF hybrids with artificial arrays of magnetic nanodots deposited on the top of superconducting films. Experiments on ordered or quasiordered arrays of dots indicate that the vortex motion is impeded when the vortex lattice becomes commensurate with the dot array, while in anisotropic arrays the opposite effect may occur when the vortex flow is channeled in some directions [22–29]. The enhancement of the critical current density by random removal of the nonmagnetic pinning sites has been reported [30], and partially explained by disorder-induced suppression of channeling predicted theoretically [31], but with some aspects of the observations still remaining unclear.

In contrast to those in fixed nanodot arrays, the magnetic domain patterns in planar SFBs can be reversibly manipulated. An example has been demonstrated in SFBs with substrate-induced magnetic domain walls [32], or with regular stripe domains [33], in which directional flux flow may be induced by the domain alignment. Previous studies have shown also that presence of domains enhances the magnetic pinning, although the effect has not been significant [34–40]. Recently, we have demonstrated large and tunable enhancement, by a factor in excess of 10, in SFBs containing F layer with perpendicular magnetic anisotropy (PMA) [12,41]. This is accomplished by angled demagnetization which defines quasiperiodic domain patterns with equal amount of $+/-$ domains with tunable domain width $w$. The enhancement is due to pinning of vortex chains by domains of one sign. The enhancement is the largest when $w$ becomes comparable to the magnetic penetration depth $\Lambda$. We note that formation of single or multiple vortex chains confined to domains of one sign has been previously evidenced by direct imaging techniques in SFBs with regular domain patterns [42,43].

The planar SFB with PMA may be employed also to study the vortex confinement by more complicated domain patterns, in which the amount of $+/-$ domains is unequal, so that isolated domains of one sign are immersed in the background of the opposite sign. Recently, we have shown that such patterns may be reversibly defined and erased using the procedure of partial magnetic reversal, so that the flux

 

penetration can be studied in a single tunable sample [44]. The results are consistently explained by the flux confinement into various vortex structures, chains or lattices, depending on the domain geometry and the amount of +/− domains.

Despite the success of these experiments, the understanding of the vortex dynamics in planar SFBs is still in the early stage. In particular, it is not clear how disorder in the domain patterns affects vortex behavior. In most of the SFBs with PMA which we have studied, to date the domain patterns are quasiperiodic. While there are well-defined average domain widths, the standard deviations differ considerably from sample to sample. In view of the effect that disorder has on the channeling in nanodot arrays [30], it may be expected that it also plays an important role in the vortex dynamics in planar SFBs, affecting possibly both the confinement of vortices and the enhancement of the magnetic pinning.

Here, we address this problem by comparing the vortex behavior in two tunable SFBs. Both SFBs are built from niobium as the S layer and Co/Pt multilayer as the F layer, but the thicknesses of Pt layers in Co/Pt are different at 0.3 nm (Pt3 sample) and 1.4 nm (Pt14 sample), which affects the shapes of tunable domains defined by the partial magnetic reversal process. In both samples, the domain patterns evolve from a maze of interconnected wide domains into a collection of well-isolated narrow domains. However, the dispersion of domain width $\Delta w$ is always substantially larger in the Pt3 sample, creating more disordered domain landscape. In addition, narrow domains break into short, unconnected pieces in the Pt3 sample, while they remain always long in the Pt14 sample. We use local (Hall sensors) magnetometry to evaluate flux confinement and the enhancement of pinning in both samples. The most interesting result is that different domain landscapes influence confinement and enhancement in quite opposite fashion, and that this influence depends on the domain width. In the range of narrow magnetic domains, the confinement is larger for strongly disordered landscape, in which $\Delta w$ is large and domains are short. On the other hand, the enhancement of the magnetic pinning reaches high values for less disordered landscape, in which $\Delta w$ is small and domains are elongated. However, the reverse is true in case when magnetic domains are wide.

## II. EXPERIMENT

### A. Sample preparation

SFBs have been made by magnetron sputtering at room temperature onto the Si substrate. The sequence of the layers is Si(10)/Pt(10)/$[Co(0.6)/Pt(h)]_8$/Si(10)/Nb(75), where all thicknesses are denoted in nm and $h$ is the thickness of Pt layers, equal to 0.3 nm (Pt3) and 1.4 nm (Pt14). The surface roughness of the Co/Pt superlattice, measured by atomic force microscopy, remains in the range 0.1 to 0.3 nm. We have checked previously [44] that the amorphous Si layer between CoPt and Nb eliminates proximity effect. The structure of samples is shown schematically in Fig. 1(a).

### B. Magnetic domain patterns

Figure 1(b) shows the hysteresis loops of the F layers of both samples measured at 300 K using a SQUID magnetometer

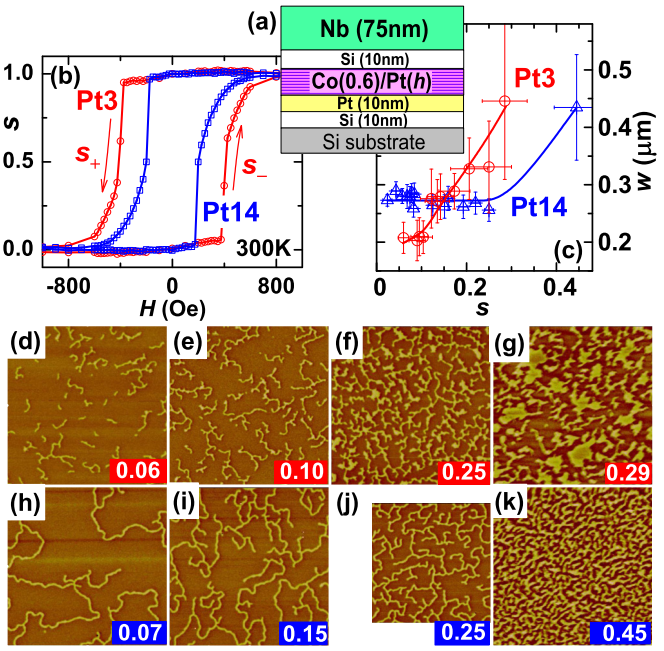


FIG. 1. (a) Schematic drawing of the SFB. $h$ equals to 0.3 and 1.4 nm in the Pt3 and Pt14 sample, respectively. (b) Hysteresis loops of CoPt measured by SQUID at 300 K. (c) Widths of domains $w$ estimated from MFM images, versus parameter $s$. (d)–(g) and (h)–(k) MFM images at 300 K, for Pt3 [(d)–(g)] and Pt14 [(h)–(k)] samples, for various $s$ states indicated by labels. The size of image (j) is 15 $\mu$m × 15 $\mu$m, the size of all remaining images is 20 $\mu$m × 20 $\mu$m.

with the magnetic field $H$ applied perpendicular to the sample surface. The vertical scale shows rescaled magnetization, which we define as $s = \frac{1}{2}(\frac{M}{M_s} + 1)$, with $M$ and $M_s$ as the magnetization and the magnetization at saturation, respectively. For the saturated F layer, $s$ is equal to 0 or 1. The coercive fields $H_C$ are 412 Oe (Pt3) and 200 Oe (Pt14) at 300 K, and they increase to 720 Oe (Pt3) and 320 Oe (Pt14) upon cooling to 10 K. The loops have almost rectangular shape, typical for Co/Pt multilayers with PMA [45], with a rapid change of the $M$ in close vicinity of $H_C$, followed by slower approach to saturation at magnetic fields exceeding $H_C$, taking a form of an extended "tail." Similar shapes of hysteresis loops may be also evidenced by the anomalous Hall effect (AHE), as illustrated in Figs. 2(a) and 2(b) for $T = 10$ K. The Hall effect data are acquired using four electrical leads attached to the sample, and the AHE data are extracted from it after subtraction of the ordinary Hall effect, estimated from high magnetic field region [46]. The Hall voltage ($R_H$) measured in saturation is by a factor of about 1.43 larger in Pt14 sample than the one in Pt3, reflecting the larger magnitude of $M_s$ in Pt14. Larger $M_s$ and smaller $H_C$ in multilayers with larger $h$ have been reported before, and attributed to the polarization of the Pt layers, and the oscillatory character of the Ruderman-Kittel-Kasuya-Yosida interlayer coupling, respectively [45].

To define the domain patterns in the F layer we use partial magnetic reversal process, as previously described [38,44]. Some of the patterns, imaged by magnetic force microscopy (MFM), are presented in Figs. 1(d)–1(k). For example, to set the domain pattern shown in MFM image in Fig. 1(f) the

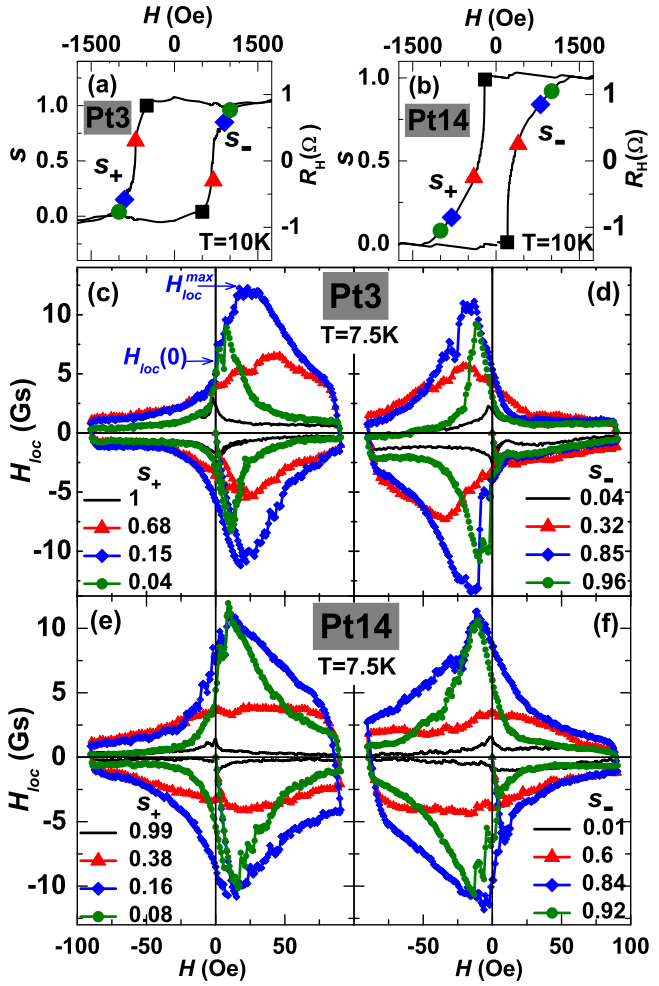


FIG. 2. Hysteresis loops measured by AHE at $T = 10$ K for Pt3 (a) and Pt14 (b). Points show the $s$ values for which the data shown in (c)–(f) are taken [color and shape coded to match data in (c)–(f)]. (c)–(f) Hysteresis loops measured at the sample center at $T = 7.5$ K, for different values of $s_+$ in Pt3 (c), $s_-$ in Pt3 (d), $s_+$ in Pt14 (e), and $s_-$ in Pt14 (f).

sample is first magnetized to saturation ($s = 1$) at 300 K, by applying large positive field $H = +2$ T. Next, the magnetic field is lowered to zero, reversed, and increased towards $-H_C$, when $s$ starts to drop. After reaching the value of $s$ of about 0.25 the increase of the field is stopped and slowly decreased to zero. The magnetization is measured during this process to monitor the relaxation, which is small provided the magnetic field is ramped slowly. After the magnetization is relaxed, the value of $s$ is calculated, the sample is moved to MFM, and the domain pattern created in the process is imaged. Since the magnetic reversal is not complete, some uninverted areas remain, creating a pattern of uninverted residual (RU) domains (bright) in mostly inverted background (dark). Domain pattern remains stable during imaging. The ratio of the surface area of RU domains to the total image area agrees very well with the value of $s$ measured by magnetometry. The polarity of the RU domains depends on which process we use to define them: they are positive (negative) for the process starting from $s = 1$ ($s = 0$). In the following, we introduce subscripts to $s$ to distinguish processes of magnetic reversal of the F layer, that is, $s_+$ ($s_-$) process is the one starting from $s = 1$ ($s = 0$). These definitions are depicted in Fig. 1(b).

MFM images shown in Fig. 1, obtained after the $s_+$ reversal process, reveal that the evolution of domain patterns with $s$ is very different for both SFBs. In case of Pt3 sample [images 1(d)–1(g)] the pattern at large $s$ ($s = 0.29$) consists of a maze of RU interconnected domains with a large spread of widths, from narrow to wide. With decreasing $s$ the domains became more uniform in widths and shorter ($s = 0.25$), break apart into separate pieces ($s = 0.1$), until eventually they become short, narrow, and well isolated ($s = 0.06$). On the other hand, images 1(h)–1(k) for Pt14 show RU domains which are long, reaching from one side of image to the other, even for the smallest $s$. The domain widths remain quite uniform for various $s$, simply the amount of RU domains changes. To quantify at least partially these observations, we have measured the RU domain width $w$ in many places along each domain in a series of images taken for various $s$. Based on this, the average $w$ and standard deviation $\Delta w$ are calculated, as shown in Fig. 1(c). We see that at small $s$ the average $w$ is smaller for Pt3 than for Pt14, while the average $\Delta w$ is by a factor of about 2 larger in Pt3 than in Pt14. With increasing $s$ both $w$ and $\Delta w$ start to increase rapidly in Pt3, while in Pt14 they remain approximately unchanged up to $s = 0.25$. We conclude that RU domain landscape in the Pt3 sample is substantially more disordered than that in Pt14. Note that the difference in the shape of RU domains in the two samples is well reflected in the shape of hysteresis loops. Namely, regardless of temperature, the loop measured for Pt14 sample shows more extended "tail" section (with respect to $H_C$) than the loop measured for Pt3. Since it is well documented that "tail" results from slow annihilation of the RU domains [47], the longer "tail" is expected when the RU domain is more uniform in shape and, therefore, more difficult to annihilate.

The origin of larger disorder of the magnetic domain pattern in case of Pt3 sample may be traced to smaller total thickness of the F layer, $d_F$, which consists of Co layers and polarized Pt layers. In case of a striped magnetic domain pattern in equilibrium (i.e., defined by demagnetization) the total energy density per unit surface area shows a minimum as a function of domain width $w$, resulting from different $w$ dependence of two contributing terms: magnetostatic energy and domain-wall energy. This minimum, which determines $w$ in the system, is deep and well defined for large $d_F$, but becomes very shallow and ill defined for small $d_F$ [48]. As a result, the increase of $\Delta w$ with decreasing $d_F$ is expected. While the partial reversal process, which we use in the present experiment, does not create equilibrium domain patterns, nevertheless, the residual domains still retain larger $\Delta w$ in case of the Pt3 sample.

Finally, we mention that the domains may shrink upon cooling down. The estimate based on the Kaplan's model [49] and the $T$ dependence of $M_s$ [33] shows that the shrinkage in the present case could reach about 30% at $T = 8$ K. Decrease of domains size is taken into consideration during further discussion. Nevertheless, we stress that the difference in the shapes of hysteresis loops is observed regardless of temperature. This indicates that the most essential difference in the RU domain shapes in both samples is not substantially altered by cooling.

### C. Superconducting properties

The superconducting transition temperature $T_c$ and the coherence length $\xi(0)$ of the Nb layers in both SFBs are $T_c = 8.56$ K and $\xi(0) = 14.5$ nm (Pt3), and $T_c = 8.50$ K and $\xi(0) = 13.4$ nm (Pt14). They are extracted from magnetoresistance measurements in perpendicular magnetic field, with a sample attached to a resistance measuring probe. Prior to the measurements, the F layers are magnetized to saturation. Using the standard formulas for superconductors in the dirty limit [50], we estimate the Ginzburg-Landau parameter $\kappa \approx 3.8$ and 4.5 for Pt3 and Pt14, respectively, the $T$-dependent magnetic penetration depth $\lambda(T) \sim \kappa\xi(0)/\sqrt{1 - T/T_c}$ and the effective penetration depth $\Lambda = \lambda^2/t_S$, where $t_S$ is the thickness of the S layer. At temperatures in our experiments, $T = 7.5$ and 7 K, $\Lambda$ is equal to about 333 and 226 nm (Pt3), and 409 and 273 nm (Pt14), respectively.

### D. Measurement procedure

To study the flux penetration in the S layer, we measure the local magnetic induction $B$ as a function of the distance from the sample edge $x$, as described in detail elsewhere [41,44]. Briefly, the measurements are performed using the line of 10 miniature Hall sensors, of the area $A_{\text{sen}} = 5 \times 5\ \mu\text{m}^2$ each, and situated 20 $\mu$m apart along a line. The sample is cut into a strip, about 240 $\mu$m wide and 3–4 mm long, which is placed with the niobium side down across a line of sensors, as shown schematically in Fig. 4(a). An additional sensor attached a few millimeters away from the sample edge measures the external magnetic field $H$ in the sample space. The measurements of $B(x)$ are done for all the sensors consecutively at each $H$ value. The arrival or exit of one flux quantum $\Phi_0 = 20.7\ \text{Gs}\,\mu\text{m}^2$, from the vicinity of a sensor of the area $A_{\text{sen}} = 25\ \mu\text{m}^2$, results in the change of the measured signal of the magnitude $\Delta B \simeq \Phi_0/A_{\text{sen}} \simeq 0.8$ Gs. In addition to the $B(x)$ profile, we extract from the data the dependence of the local magnetic field, defined as $H_{\text{loc}} = B - \mu_0 H$, on the external magnetic field. As has been discussed previously [44], the curve $H_{\text{loc}}(H)$ measured at the sample center resembles the hysteresis loop usually registered by global magnetization measurements.

To evaluate the influence of domains on the flux pinning, we proceed as follows. First, the RU domain pattern in the F layer is predefined at $T = 10$ K, using the partial magnetic reversal process described above. The value of $s$ is monitored by the AHE measurement, using four separate electrical leads. After the domain pattern is defined, the magnetic field is removed, and the sample is cooled just below $T_c$. The measurements of $B(x)$ are done for all the sensors while the external magnetic field is cycled. The maximum $H$ is kept below $\pm 90$ Oe. We have verified that this small magnetic field (much smaller than $H_C$ for both samples) does not affect domain pattern.

## III. EXPERIMENTAL RESULTS

### A. Enhancement of pinning

Figures 2(a) and 2(b) show the hysteresis loops measured by AHE at $T = 10$ K for Pt3 and Pt14 samples. Points indicate several different values of $s_+$ and $s_-$ predefined at $T = 10$ K, for which the hysteresis loops are subsequently measured below $T_c$. The hysteresis loops registered by the sensor at the sample center at $T = 7.5$ K are shown for the Pt3 and Pt14 samples in Figs. 2(c) and 2(d) and 2(e) and 2(f), respectively. There are some characteristic features present, similar in case of both samples. First, the peak-to-peak widths of the loops, measured in the saturated states ($s_- = 0$ or $s_+ = 1$), shown by black lines, are the smallest. These loops are also relatively smooth, with occasional flux jumps not exceeding 1 Gs. When the RU domains are predefined and $s$ differs from 0 or 1, the widths of the hysteresis loops increase, suggesting enhanced pinning induced by the RU domains. Moreover, the magnitude of flux jumps increases substantially, with some of them exceeding 10 Gs or more. We have shown recently that such a feature indicates nonuniform flux propagation inside the sample triggered by RU domains [44]. Second, when the RU domains are present the hysteresis loops become strongly asymmetric. Specifically, when the positive RU domains are predefined in the $s_+$ process, the enhancement of pinning is strong at positive $H$ [Figs. 2(c) and 2(e)], whereas $s_-$ process results in the enhancement mostly at negative $H$ [Figs. 2(d) and 2(f)]. This shows that the pinning enhancement is large when the polarities of vortices and RU domains are the same, exactly as it is expected in case of magnetic pinning of vortices by RU domains [1,6,14,38,39,44].

In addition to the similarities mentioned above, there are two prominent differences between hysteresis loops for the two SFBs. These differences are the main focus of this paper. One of them is the magnitude of the pinning enhancement, which is very different in the two SFBs. To discuss this, we define the quantity which may be used as a measure of the pinning enhancement $G = \Delta H_{\text{loc}}/\Delta H_{\text{sat}}$, where $\Delta H_{\text{loc}}$ and $\Delta H_{\text{sat}}$ are the widths of the hysteresis loop (registered by the sensor at the sample center) of the SFB with predefined RU domains and that with the saturated F layer, respectively. These quantities are depicted in the inset to Fig. 3(a), where the data are for the Pt3 sample measured at $T = 7.5$ K. We have shown in our previous studies [41,44] that $G$ provides a good estimate of the pinning enhancement.

The dependence of $G$ on $s_+$ is shown in Fig. 3(a) for the Pt3 and the Pt14 samples at two different temperatures (similar results, mirror reflected with respect to $s$ value, are obtained for the $s_-$ process). We note first that all curves show a qualitatively similar shape, with a broad maximum of $G$ at small $s$, and a gradual decrease of $G$ towards 1 for large $s$. The largest value of $G$, of about 7.2, is observed in the Pt14 sample at highest temperature, whereas the maximum $G$ in Pt3 is about 4.3, that is, by a factor of 1.7 smaller. It is tempting to attribute this difference to a larger magnetic field created by domains in the Pt14 sample, as evidenced by the larger $M_s$ value. However, in Fig. 3 we observe other features, which cannot be attributed to a larger magnetic field.

One of these features is a strong dependence of $G$ on $s$, which correlates with the evolution of the magnetic domain patterns. The initial increase of $G$ with increasing $s$, followed by a maximum of $G$, appears in both samples. It is likely that this initial increase of $G$ is caused by the increase of the surface area of RU domains, as evidenced by MFM images. As $s$ exceeds about 0.2, the $G$ is suppressed, particularly rapidly in the Pt14 sample, in which $G$ approaches 1 for $s \gtrsim 0.5$, indicating that the enhancement of pinning becomes insignificant. We remark that this does not mean

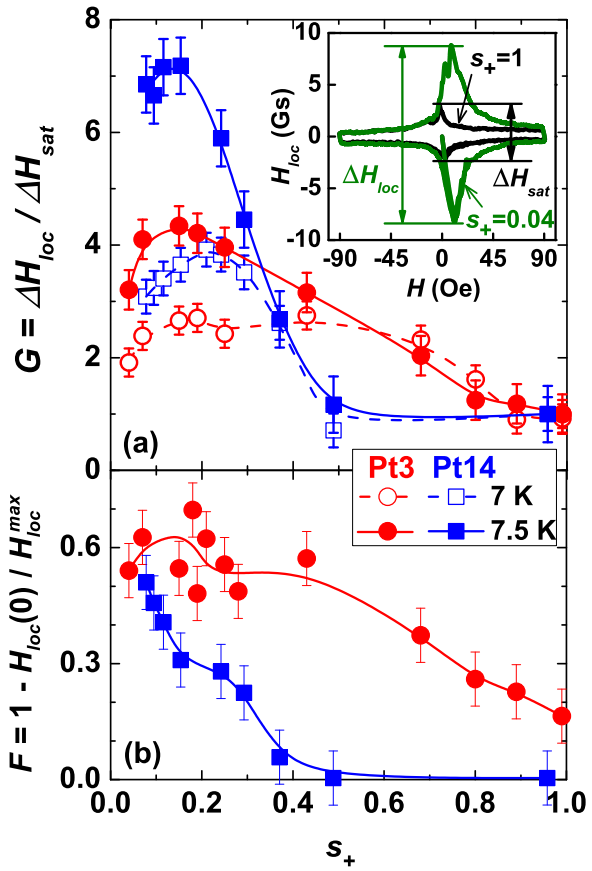


FIG. 3. (a) $G = \Delta H_{\rm loc}/\Delta H_{\rm sat}$ versus $s_+$ for $T = 7.5$ K (full points, solid lines) and $T = 7$ K (open points, dashed lines) for Pt3 (red circles) and Pt14 (blue squares). Inset: definitions of $\Delta H_{\rm loc}$ and $\Delta H_{\rm sat}$; the data are for Pt3 at $T = 7.5$ K. (b) $F = 1 - H_{\rm loc}(0)/H_{\rm loc}^{\rm max}$ versus $s_+$ at $T = 7.5$ K for Pt3 (red circles) and Pt14 (blue squares). The definitions of $H_{\rm loc}^{\rm max}$ and $H_{\rm loc}(0)$ are illustrated in (c). All lines are guides to the eye.

that the magnetic pinning disappears for $s \gtrsim 0.5$. The shape of hysteresis loop in this region is very different from the shape for saturated sample: the loop lacks the sharp maxima at $H = 0$. This indicates that the flux dynamics is affected by magnetic pinning.

A probable origin of the $G$ suppression may be the increasing width of RU domains. As domains become wide, they become less effective pinning centers because the magnitude of the magnetic field at the domain center scales in inverse proportion to the domain width [51]. However, note that the decrease of $G$ is much faster in case of the Pt14 sample, while the domain width increases faster in Pt3. Therefore, the reduction of the vortex-domain interaction with increasing $w$ cannot solely explain the suppression of $G$. Looking for other possible reasons, we note that the domain patterns in the two samples differ by the magnitude of $\Delta w$. Large $\Delta w$ in the Pt3 sample likely leads to inhomogeneous distribution of vortices, which are weakly trapped in some areas of the sample, and much more strongly trapped in other areas. The net effect is the substantial enhancement of pinning, which persists at large $s$. On the other hand, $w$ is very uniform across the Pt14 sample, and facilitates the easy flow of vortices along domains. We speculate that, as a result, in the Pt14 sample at large $s$ the arrangement of vortices above the domain pattern becomes mainly dependent on vortex-vortex interactions, so it differs little from the arrangement in the absence of magnetic domains.

Still another feature, which indicates the important role of domain geometry, is the $T$ dependence of $G$. We observe that the lowering of temperature has quite distinct effects on $G$ in the small-$s$ and in the large-$s$ regions. Specifically, with the decrease of $T$, the maximum of $G$ at small $s$ is suppressed in both samples; the boundary of this low-$s$ region is located at $s \approx 0.45$ (Pt3), and $s \approx 0.35$ (Pt14). On the other hand, at larger $s$ the magnitude of $G$ is unaffected by temperature. Since $G$ is a ratio of two quantities $\Delta H_{\rm loc}$ and $\Delta H_{\rm sat}$, we may estimate the $T$ dependence of $\Delta H_{\rm loc}$ in the small-$s$ range based on the measured $T$ dependence of $\Delta H_{\rm sat}$ in saturated sample. We find that the lowering of $T$ from 7.5 to 7 K results in the increase of $\Delta H_{\rm sat}$ by a factor of about 2.8 and 2.6 in the Pt3 and Pt14 samples, respectively [most likely as a result of the decreasing coherence length, the size of which becomes slightly closer to the intrinsic (nonmagnetic) defect size as $T$ decreases]. It follows that in the same $T$ range and at small $s$, the $\Delta H_{\rm loc}$ increases by a factor of about 1.7 (Pt3) and 1.4 (Pt14), which is a weaker increase than that of nonmagnetic pinning. On the other hand, at large $s$ the increase of $\Delta H_{\rm loc}$ is similar to that of $\Delta H_{\rm sat}$. Thus, the magnetic pinning not only shows strong dependence on $s$, it also shows quite distinct $T$ dependencies in the small-$s$ and in the large-$s$ regions.

So far, we have described the difference between the $G(s)$ dependencies in Pt3 and Pt14 samples. The second difference in the flux behavior for these two samples is more subtle, and it is related to the efficiency of the flux expulsion from the sample when the external magnetic field decreases to zero and changes sign. The notable observation is that the expulsion is less rapid in case of the Pt14 sample, so that larger flux remains pinned when $H$ reaches zero value. To explain this, we focus on top (positive) branch of the hysteresis loop measured in the $s_+$ process [Figs. 2(c) and 2(e)]. When the external magnetic field is decreased from +90 Oe towards −90 Oe, first a maximum of $H_{\rm loc}$ is reached. This value, labeled $H_{\rm loc}^{\rm max}$, is indicated by the arrow in Fig. 2(c) on the blue curve measured for $s_+ = 0.15$. This is followed by a rapid decrease of $H_{\rm loc}$ resulting from flux expulsion. In Fig. 2(c), we mark by a second arrow the value $H_{\rm loc}(0)$ when the external field $H$ reaches zero. Thus, the normalized quantity $F \equiv 1 - H_{\rm loc}(0)/H_{\rm loc}^{\rm max}$ measures what portion of total flux pinned in the sample is expelled from it when $H$ decreases to zero.

Figure 3(b) shows $F$ for both SFBs, extracted from the data taken in $s_+$ process at $T = 7.5$ K (similar results are observed at lower $T$). Except for the data at smallest $s$, when the values of $F$ within error bars are comparable in the two samples, all other data clearly show significantly smaller values of $F$ in the Pt14 sample, indicative of slower flux expulsion. One may try to associate this result with the larger magnetic field emanating from the domains in Pt14. However, such explanation is inconsistent with the strong $F(s)$ dependence. Namely, when $G$ is reduced for $s \gtrsim 0.15$, the $F$ is reduced as well. This occurs in case of both samples, but it is particularly well visible in case of the Pt14 sample. Thus, the decrease of the pinning enhancement is accompanied by slowing of

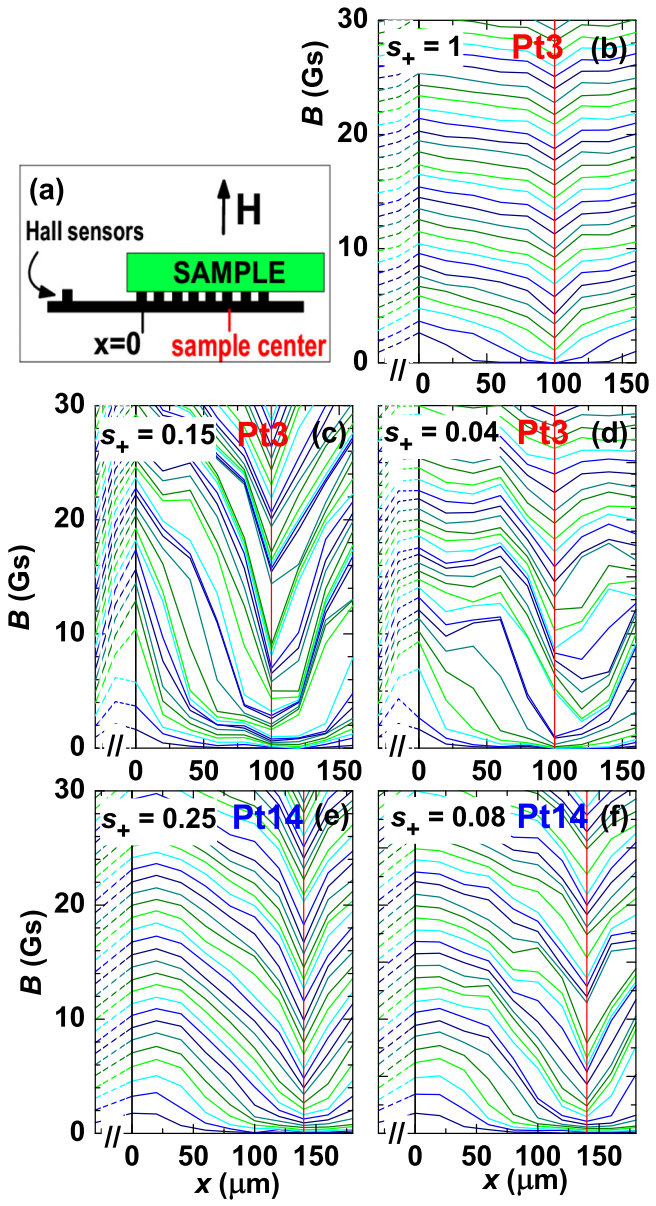


FIG. 4. (a) The line of Hall sensors with Nb on the top. (b)–(f) The profiles $B(x)$, for Pt3 sample with $s_+$ equal to 1 (b), 0.15 (c), and 0.04 (d); and for Pt14 sample with $s_+$ equal 0.25 (e), and 0.08 (f). All data are accumulated at $T = 7.5$ K.

the flux expulsion. We will come back to discuss this point later.

### B. Flux penetration

In an effort to understand more details of the flux dynamics, it is useful to analyze the full profile of the magnetic induction measured across the sample $B(x)$. Several such profiles, measured at $T = 7.5$ K during the initial sweep of $H$ from 0 to +30 Oe, are shown in Fig. 4. The data in Fig. 4(b) are for the Pt3 sample magnetized to saturation (the data for Pt14 are very similar), while Figs. 4(c) and 4(d) and 4(e) and 4(f) show data for two different values of $s_+$ for Pt3 and Pt14 samples, respectively. Two vertical lines, black and red, indicate the data accumulated by sensors closest to the sample edge ($x = 0$) and to the sample center, respectively, as shown schematically in Fig. 4(a). The data on the left vertical axis show the $H$ value measured in the sample space. The centers of two samples are at different $x$ because the widths of the samples differ.

The $B(x)$ dependencies measured for saturated F layer [Fig. 4(b)] are close to the linear. This disagrees with the theoretical predictions for thin films with field-independent critical current density [52–56], according to which large nonlinearity at the sample edge is expected. However, we have shown previously that $J_c$ is not field independent in these samples [44]; in addition, the finite resolution of our experiment may wipe out nonlinearities.

When positive RU domains are predefined, the profiles change dramatically. Two main changes may be noted. First, large accumulation of flux appears in the vicinity of the sample edge, and, as a result, the flux penetration towards the sample center is delayed. Second, the slope of $B(x)$ increases strongly, which points to the increase of the $J_c$. These effects are, however, very different in the two SFBs. The $B(x)$ measured in the Pt3 sample exhibits abrupt changes of slope, from large to small, indicating very nonuniform distribution of the $J_c$ across the sample [Figs. 4(c) and 4(d)]. The accumulation of flux close to the sample edge is large, particularly when $s_+ = 0.15$. This behavior is very similar to the one which we have studied and thoroughly discussed in the previous paper [44]. It signals strong confinement of vortices by RU domains. On the other hand, the profiles for the Pt14 sample, shown in Figs. 4(e) and 4(f), are much more smooth, with gradual increase of the slope towards the sample center. Moreover, the flux accumulation at the sample edge is rather modest. These observations suggest that in the Pt14 sample the $J_c$ is spatially more uniform, and the confinement of vortices is weaker in comparison with the Pt3 sample.

To compare more quantitatively the behavior of flux in the two SFBs, we follow the procedure outlined in Ref. [44]. First, we consider the dependence $H_{\rm loc}(H)$, measured by a sensor situated closest to the sample edge (at $x = 0$). Several examples of this dependence, measured for two SFBs with various $s_+$ at $T = 7.5$ K, are displayed in Fig. 5. We observe that with increasing $H$ the $H_{\rm loc}$ initially increases faster than $H$, exhibits a maximum at certain $H = H_0$, and subsequently slowly decreases. The magnitudes of maximum of $H_{\rm loc}$ at $H_0$, and $H_0$ itself, are very small in saturated samples (and comparable in both of them), but they strongly increase in the presence of RU domains. As an example, in Fig. 5 we mark by black arrows the positions of $H_0$ in saturated samples, while red arrows show $H_0$ for $s_+ = 0.15$ (Pt3) and $s_+ = 0.12$ (Pt14). It has been demonstrated [44] that the maximum of $H_{\rm loc}(H_0)$ is associated with a change of slope on the dependence of $B(H)$, situated at the same $H_0$. This change of slope indicates that for $H \lesssim H_0$ the flux is accumulated in the vicinity of the sample edge, while for $H \gtrsim H_0$ it starts to transfer towards inside the sample when strong vortex-vortex interactions push vortices inside. The accumulation of flux in the initial stages of flux penetration is usually attributed to demagnetization effects which lead to compression of flux lines close to a border of thin film placed in perpendicular magnetic field [55]. Our experiment indicates a dramatic increase of the flux accumulation in the presence of RU

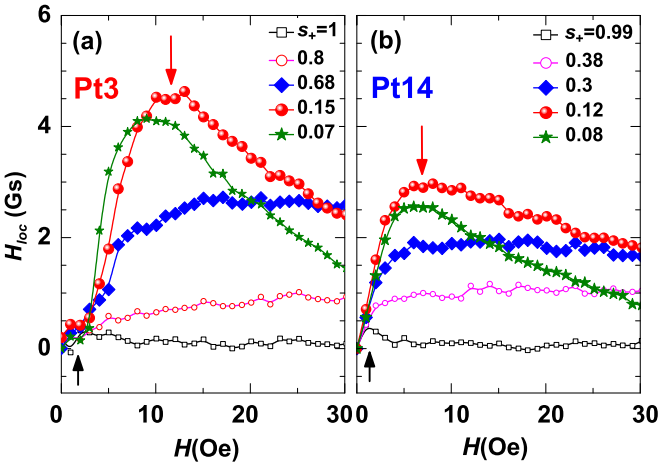


FIG. 5. $H_{loc}$ versus $H$ at $x = 0$ and $T = 7.5$ K for various $s_+$, measured in Pt3 (a) and Pt14 (b) samples. The black arrows indicate the $H_0$, the positions of the maxima on $H_{loc}$ curves, in case of saturated samples, while red arrows show $H_0$ for $s_+ = 0.15$ (a) and $s_+ = 0.12$ (b).

domains, signaling enhanced demagnetization which results from the enhancement of the vortex pinning.

The magnitude of the accumulated flux density, just before it starts to transfer towards inside the sample, may be estimated from the value of $B(H = H_0)$. The corresponding density of vortices is given by $n = B(H_0)/\Phi_0 = [H_{loc}(H_0) + \mu_0 H_0]/\Phi_0$. In Fig. 6, we show the dependencies $n(s)$ (in the $s_+$ process), extracted from the data for both SFBs and for two temperatures. It is seen that $n$ strongly depends on $s$. All curves show the initial increase of $n$ at small $s$, followed by a maximum, and subsequent decrease in the large-$s$ range. The initial increase of $n$ is similar to the initial increase observed in $G(s)$, and the maxima occur at approximately the same $s_+$ value as the maxima observed in the $G$ [Fig. 4(a)]. Moreover, the decrease on $n$ at large $s$ is very rapid in case of the Pt14 sample, and much more gradual in Pt3, just as it is observed in case of $G$.

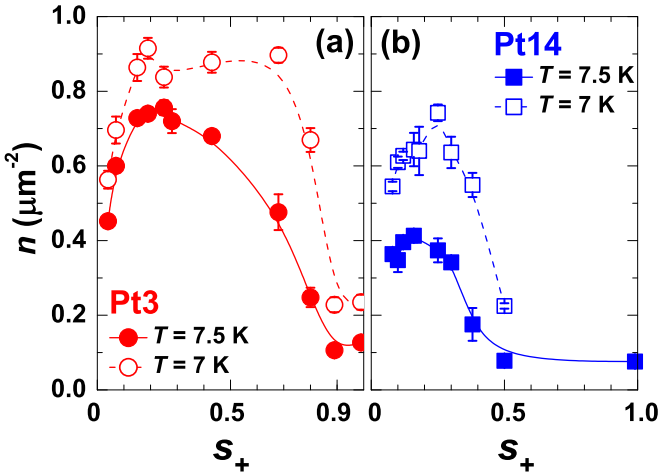


FIG. 6. $n$ versus $s$ in the $s_+$ process in Pt3 (a) and Pt14 (b) samples. The data are obtained at $T = 7.5$ K (full points, continuous lines) and 7 K (open points, dashed lines). All lines are guides to the eye.

The correspondence between $n(s)$ and $G(s)$ indicates that $n$ reflects the geometry of the magnetic domain pattern, just as the $G$ does. This is not surprising. As we have thoroughly discussed in the previous work [44], $n$ is a density of vortices present in the vicinity of the first sensor when the density of *trapped* flux reaches a maximum, just before the combined effects of self-field and magnetic pinning by RU domains is overcome by the vortex-vortex interaction which push vortices towards sample center. In the initial stage of flux penetration, the vortices are known to fill up the potential minima created by the pinning centers; this has been demonstrated recently by scanning Hall microscopy of Pb film with ordered arrays of antidots on top [57]. It is reasonable to expect that a similar phenomenon occurs in case of SBFs, in which vortices fill the potential minima created by RU domains. Thus, the behavior of $n(s)$ reflects the geometry of RU domain patterns.

Interestingly, there is an important difference between $n(s)$ and $G(s)$ dependencies. Namely, the maximum magnitude of $n$, observed in the small-$s$ range, is larger in the Pt3 sample, while the maximum value of $G$ occurs in the Pt14. To explain this anticorrelation between $n$ and $G$, observed at small $s$, we recall that these quantities measure different properties. While $G$ describes the enhancement of flux pinning induced by RU domains inside the whole sample, from the edge to the center, and in the presence of large flux density, the $n$ represents the density of vortices in the vicinity of the sample edge during the initial flux entry. When the flux first enters the sample, the vortices are confined to the potential minima created by RU domains. In the small-$s$ range ($s \lesssim 0.15$), the magnetic domains are narrow and short in the Pt3 sample, therefore, the flux is very effectively trapped by these domains. On the other hand, in the Pt14 sample the domains are wider, moreover, they are long. Therefore, the vortices flow along these domains easily, which diminishes the confinement. Note that even if the stray magnetic fields created by domains are larger in the Pt14 sample (as suggested by larger $M_s$ value), the elongated domains do not produce as effective confinement of vortices as short domains do. As a result, $n$ is larger in the Pt3 and smaller in the Pt14 sample. Furthermore, the weaker confinement of vortices at the edge of the Pt14 sample contributes to more effective flux propagation towards sample center, resulting in larger magnitude of $B$ in the center at the same value of the $H$. Thus, the elongated shape of magnetic domains contributes to the larger $G$ measured across the Pt14 sample.

When $s$ increases above 0.15, the RU domains in the Pt3 sample become on average wider than the domains in Pt14. However, the domain pattern remains more disordered in the Pt3 sample, with many narrow domains which inhibit easy vortex flow. Therefore, even at larger $s$ the disordered vortex pattern contributes to larger $n$ in the Pt3 sample. As we have already mentioned, the presence of disordered domain pattern contributes also to relatively large values of $G$ in the range of large $s$ in the Pt3 sample. The situation is different in the case of the Pt14 because increasing interconnections between domains, combined with very uniform domain width, results in enhanced vortex flow. Thus, both $n$ and $G$ are strongly suppressed at large $s$ in the Pt14 sample.

Finally, the $T$ dependence of $n$ testifies that the behavior of magnetic pinning is different in the small-$s$ and large-$s$ regions. Specifically, while Fig. 6 shows that the decrease of $T$

results in increase of $n$ for all $s$ values, the increase is relatively small in the range of small $s$, i.e., by a factor of about 1.2 for $s_+ \lesssim 0.45$ (Pt3) and by a factor of about 1.7 for $s_+ \lesssim 0.35$ (Pt14). On the other hand, at larger $s$ the increase is by a factor well exceeding 2 in both samples. This may be compared to the results inferred from the $T$ dependence of $G$ which we have already described, from which we estimate in the same $T$ range an increase of $\Delta H_{\rm loc}$ by a factor of about 1.7 (Pt3) and 1.4 (Pt14) at small $s$, and by a larger factor (comparable to the increase of nonmagnetic pinning) at large $s$. Thus, the difference between small- and large-$s$ ranges is confirmed. Note that the magnitudes of $T$-induced changes of $n$ and $\Delta H_{\rm loc}$ in the small-$s$ range affirms the existence of the anticorrelation between these quantities, i.e., small change of flux trapped at the edge ($n$) is accompanied by large change of flux detected across the whole sample ($\Delta H_{\rm loc}$), and vice versa. What is interesting is the fact that the decrease of $T$ produces smaller change of $n$ (by a factor 1.2) in the Pt3 sample relative to Pt14 (1.7). We believe this is related to the geometry of magnetic domains. Since narrow and short domains in the Pt3 sample provide much stronger confinement for vortices than the long domains in Pt14 do, the decrease of $T$, which increases $v$-$v$ interactions, should affect more strongly the density of vortices trapped at the edge of the Pt14 sample.

## IV. DISCUSSION

So far, we have described differences between magnetic pinning observed in Pt3 and Pt14 samples, and we have listed several possible origins of these differences. These include (a) different magnitude of vortex-domain interaction in these samples, resulting from different $w$ dependence and different magnitude of the stray field, and (b) the influence of the magnetic domain landscape on the interplay between vortex-domain and vortex-vortex interactions, which may either enhance or suppress the vortex confinement and vortex flow. In this section, we discuss in more detail what might be the relative role of these effects.

### A. Vortex-domain interaction

The exact calculation of the energy of the vortex-domain system in the SFB should include several terms (vortex self-field, vortex-vortex, vortex-domain, and magnetic terms) [1] and would be quite complicated. Since we are interested in a qualitative estimate of the difference in vortex-domain interactions in the two SFBs, we consider only vortex-domain term, and we use a simple one-dimensional model shown schematically in Fig. 7(a). The system consists of the S and F layers, of thicknesses $t_{\rm S}$ and $t_{\rm F}$ ($t_{\rm S}$,$t_{\rm F} \ll \Lambda$), separated by an insulating layer of the thickness $a$. We assume that the magnetic domain pattern in the F layer consists of periodic stripe domains of the width $w$, aligned in the $y$ direction. The easy magnetization axis is parallel to the $z$ axis and the domain-wall thickness is much smaller than $w$. Most of these assumptions are valid in our experiment, except for the domain pattern, which in our SFBs is not periodic (at small $s$ not even quasiperiodic), and we will comment on this in the following. For such system the magnetization of the F layer may be described by the steplike function, hence, the $z$ component of

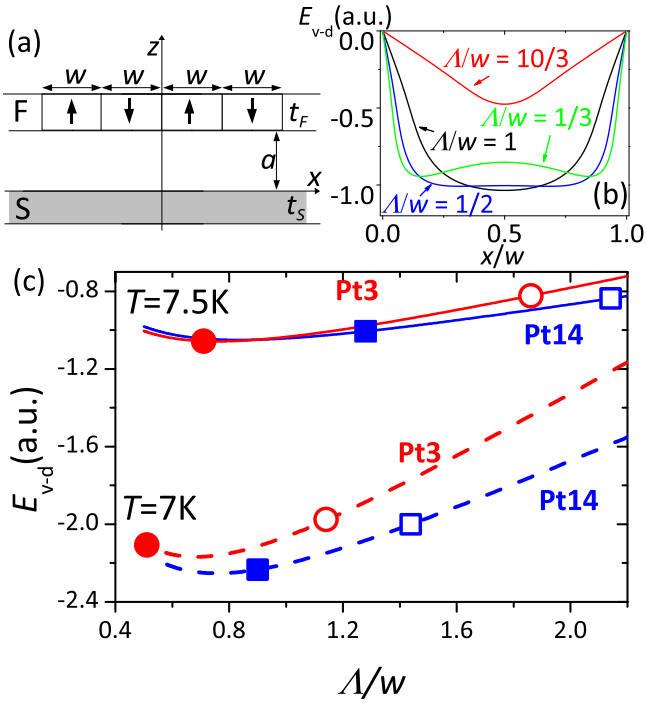


FIG. 7. Calculation of the vortex-domain interaction energy as described in Sec. IV A. (a) The system considered in the text: F and S layers separated by a buffer of thickness $a$. (b) Profile of the energy of vortex-domain interaction across the magnetic domain of the width $w$ for various ratios $\Lambda/w$. (c) Energy of vortex-domain interaction at $x = 0.5w$ for Pt3 (red lines and circles) and Pt14 (blue lines and squares) at $T = 7.5$ K (solid lines) and $T = 7$ K (dashed lines). Open symbols correspond to $s_+ = 0.15$ and close to $s_+ = 0.45$.

magnetic field distribution at the surface of the S layer ($z = 0$) is given by [51]

$$H_z(x,z=0) = \frac{4\pi m \cosh\left(\frac{\pi a}{w}\right)}{w} \frac{\sin\left(\frac{\pi x}{w}\right)}{\sin^2\left(\frac{\pi x}{w}\right) + \sinh^2\left(\frac{\pi a}{w}\right)}, \quad (1)$$

where $m$ is a magnetic moment per unit area.

To estimate the energy of the interaction between domain magnetic moment and the vortex, we use the following expression:

$$E_{v-d}(x) \propto -\int H_z(x') B_v(|x-x'|) dx', \quad (2)$$

where $B_v(|x-x'|)$ is the magnetic field at the point $x'$ from a single vortex placed at $x$. In bulk material, $B_v(r) = \Phi_0/(2\pi\lambda^2) K_0(r/\lambda)$, where $K_0(r)$ is the zeroth-order Hankel function [50]. In thin films ($t_S \ll \lambda$) the function $K_0(r/\lambda)$ should be substituted by $H_0(r/\Lambda) - Y_0(r/\Lambda)$, with $H_0$ and $Y_0$ being the Struve function and the Bessel function of the second kind, respectively. However, since $K_0(x)$ and $H_0(x) - Y_0(x)$ have the same dependence on $x$ for small distances, and the largest contribution to the integral in (2) comes from small distances $|x - x'| < w$, we use the following expression for the vortex field: $B_v(r) = \Phi_0/(2\pi\Lambda^2) K_0(r/\Lambda)$. The integration range in our calculation is restricted arbitrarily to the area $(x - 5\Lambda, x + 5\Lambda)$. Finally, note that the assumed periodic domain structure has small impact on the energy. This is

because when $\Lambda/w < 1$, the product $H_z B_v$ in (2) is close to zero for $|x - x'| > w$; on the other hand, when $\Lambda/w > 1$, there is sizable oscillatory contribution to the product $H_z B_v$, however, when integrated, this should almost cancel out.

The dependencies of $E_{v-d}$ on $x/w$ for several values of the ratio $\Lambda/w$ are shown in Fig. 7(b). For $\Lambda/w \gg 1$, the vortex has the lowest energy at $x/w = 0.5$. Therefore, omitting the vortex-vortex interactions for the low magnetic fields, the vortices will tend to form a single vortex chain along the middle of the domain. With increasing $w$, the minimum initially deepens. This is because the largest contribution to the integral (2) originates from the area of the width $w$. However, with further increase of $w$, when $\Lambda/w$ decreases below 1, the $H_z$ in the middle of the domain is suppressed. This leads eventually, above some critical domain width $w_D$ (i.e., below some critical $\Lambda/w_D$), to the appearance of two energy minima close to domain boundaries. Thus, for $w > w_D$ the vortices would have a tendency to arrange into two vortex chains close to domain walls. Based on this calculation, $w_D$ should be equal to about 0.49 $\mu$m at 7 K (in Pt3 and Pt14 samples alike), and about 0.6 $\mu$m (Pt3) and 0.65 $\mu$m (Pt14) at 7.5 K.

In Fig. 7(c), lines show the dependencies of $E_{v-d}$ at the domain center on the value of $\Lambda/w$, calculated for two SFB's and for two temperatures. We use fixed $\Lambda$ (determined from experiment at each $T$) while $w$ is varied. Open and closed symbols correspond to the experimental parameters at $s_+ = 0.15$ and 0.45, respectively. Note first that the decrease of $\Lambda$ resulting from the lowering of temperature from 7.5 to 7 K leads to significant increase of the $|E_{v-d}|$ for both samples, by a factor of about 2.4, almost independent of $w$. Interestingly, at fixed $T$ the energy is nearly the same for the two SFBs, despite the fact that the magnetic moment of the Pt14 sample is larger. This is because the larger magnetic moment is compensated by the larger value of $\Lambda$ in the Pt14 sample. Second, the dependence of $E_{v-d}$ on $\Lambda/w$ has a minimum at intermediate $\Lambda/w$, and increases both for large and for small $\Lambda/w$, in accordance with the behavior depicted in Fig. 7(b) for $x/w = 0.5$. However, this increase is rather small, the largest increase does not exceed 10% value of $E_{v-d}$.

Comparing these estimates to our experiment, we may draw the following conclusions. First, while the $T$ dependence of the $|E_{v-d}|$ explains the increase of magnetic pinning with lowering of $T$, it does not account for the fact that the increase depends on $w$, and it is weaker at small $s$. Second, larger magnetic moment in the Pt14 sample is not responsible for the differences in pinning observed in the two SFBs. Finally, the influence of the $w$ on the vortex-domain interaction is fairly insignificant, and cannot explain the dependence of the magnetic pinning on $s$. These unexplained observations must result from the interplay of the factors which are not included in our estimate, such as the two-dimensional dynamics influenced by the geometry of magnetic domains (which restricts or allows vortex flow), and the vortex-vortex interactions, which strongly depend on this geometry.

### B. Role of magnetic domain landscape

To understand the influence of the magnetic domain landscape on the interplay between vortex-domain and vortex-vortex interactions, it is useful to consider the possible

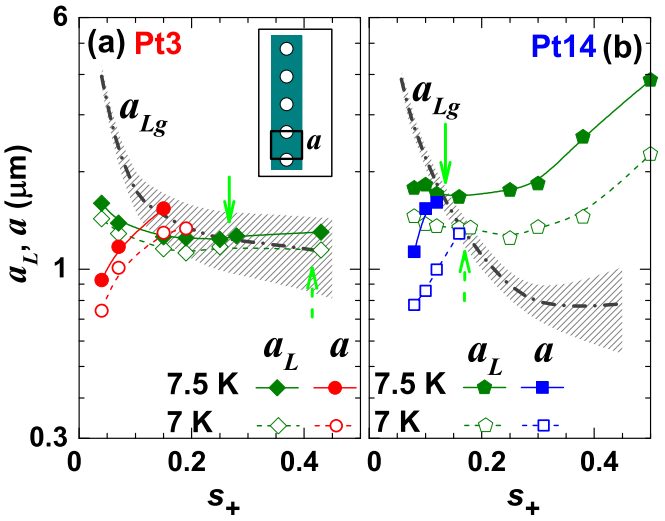


FIG. 8. The $v$-$v$ distances in the vortex lattice ($a_L$) and in the vortex chains ($a$) calculated from the vortex density $n$, measured in $s_+$ process at $T = 7.5$ K (full points, solid lines) and at $T = 7$ K (open points, dashed lines) for Pt3 (a) and Pt14 (b). All lines are guides to the eye, the experimental errors are smaller than the point size. In both figures, the thick dashed line marked "$a_{Lg}$" and the hatched area indicate the average Abrikosov lattice constant and its standard deviation, respectively, allowed by the domain geometry. The vertical arrows mark the lower boundary of the vortex lattice region, as described in the text. The inset in (a) shows schematic vortex pattern in the vortex chain.

arrangements of the vortices confined to RU domains, which would be compatible with the measured $n(s)$ dependence. We have done such analysis previously in case of different SFB, and here we follow a similar procedure [44]. We consider two simplest arrangements of vortices confined by RU domains: distorted Abrikosov vortex lattice and vortex chains.

Distorted vortex lattice may be formed when vortices pinned by neighboring RU domains are correlated. Since the domain patterns are random in our SFBs, we expect that correlations occur on a local scale, resembling somewhat the situation which has been observed in quasiperiodic magnetic pinning arrays [29]. To evaluate if such lattice formation is possible, we use the experimental data for $n$ to estimate the average lattice constants $a_L$ for the triangular lattice $a_L^2 = (4/3)^{1/2}/n$ (we limit our considerations to $s_+$ process with $s < 0.5$, which is the region with the largest $n$ and $G$). In Fig. 8, we show by green points the resulting dependencies of $a_L(s)$, calculated for Pt3 and Pt14 samples for two temperatures. Since $n$ is smaller in the Pt14 sample in comparison to Pt3, the resulting lattice constants $a_L$ are larger in Pt14; the decrease of temperature reduces $a_L$ in both samples. Next, we compare these $a_L$ values to the requirement imposed by the domain geometry. To do this, we calculate the lattice constant for the perfect triangular lattice which could be pinned by the RU domains with the width $w$ and the distance between domains $d$, $a_{Lg} = 2(d + w)/\sqrt{3}$. The distance between domains is given by $d = w(1 - s)/s$ [this is obtained from the ratio of the surface area of RU domains to the total area $s = w/(w + d)$]. From this, the above requirement for the lattice constant imposed by domain geometry reads as $a_{Lg} = 2w/(\sqrt{3}s)$. In

case of random domain pattern, this $a_{Lg}$ should be treated as average value, and from the standard deviation $\Delta w$ we can estimate the standard deviation $\Delta a_{Lg}$. In Fig. 8, we plot the dependencies $a_{Lg}(s)$ for both samples by dashed-dotted, black lines; $\Delta a_{Lg}$ is marked in both cases by hatched area. The hatched area is much larger in the Pt3 sample as a result of larger $\Delta w$.

Figure 8 reveals that in case of both samples $a_{Lg}$ is large at small $s$, and gradually decreases with increasing $s$, reflecting the fact that the distances between RU domains gradually decrease because RU domains become wider and less distant. Thus, at large $s$ we observe $a_{Lg} \lesssim a_L$, suggesting that the vortices may arrange themselves into disordered lattice. On the other hand, at small $s$ we have $a_{Lg} \gg a_L$, which indicates that lattice with the vortex density $n$ cannot be formed, and the vortices pinned by neighboring domains are not correlated. The value of $s$, at which $a_{Lg} = a_L$, may be identified as a low boundary of the vortex lattice region; we will call it $s_L$. In Fig. 8, we show by vertical (green) arrows the values of $s_L$ at 7.5 and 7 K for both samples.

Since in neither sample in the region of small $s$ the vortices pinned by neighboring RU domains may form a lattice, we consider instead another arrangement of vortices, vortex chains, confined exclusively to the RU domains, and correlated within each RU domain area. The confinement of vortices into vortex chains has been directly observed by STM imaging of $NbSe_2$/permalloy bilayer with the ordered stripe domains [42], we have also inferred a formation of vortex chains from the magnetoresistance measurements [12]. The inset to Fig. 8(a) shows schematically the pattern of vortex chain, where $a$ denotes the $v$-$v$ distance in the chain (according to considerations of the previous section, at small $s$ we do not expect a formation of double vortex chains). Using the experimental values of $n$, we can calculate the average value of $a$. From the geometry of the chain pattern it follows that the average area per vortex is $aw$, so that the vortex density inside chain areas is $1/aw$. Next, we note that the sensor, which we use to measure $n$, averages over RU domain areas (which contain vortices) and the areas without vortices (interdomain areas), while in fact all vortices occupy exclusively domain areas. Therefore, the density of vortices confined to domains is larger than $n$, it is given by $n/s$. From the equation $n/s = 1/aw$ we obtain $a = s/(nw)$. The dependence of $a$ on $s$ in the small-$s$ range is shown in Fig. 8 for both samples and for two temperatures.

Now, we can identify the important similarities and differences between the vortex patterns induced by domains in the two samples. In both cases, we expect a transition from vortex chain to vortex lattice regions at the $s_L$, as marked by green arrows; moreover, in both cases the lowering of $T$ increases $s_L$. However, the values of $s_L$ are markedly smaller in case of the Pt14 sample, which results from larger $a_L$ values, which, in turn, results from weaker vortex confinement (smaller $n$). Note also that in this case all three distances $a_L$, $a_{Lg}$, and $a$ become comparable to each other in the vicinity of $s_L$. Thus, the $v$-$v$ distance in the chains matches the lattice constant of triangular vortex lattice allowed by RU domain geometry, and also matches the lattice constant in the Abrikosov vortex lattice with the density $n$. This suggests that in the Pt14 sample in the vicinity of $s_L$ the vortices become simultaneously correlated both inside the chains and between neighboring RU domains. Moreover, the locations of $s_L$ are quite close to the positions of the maxima on the $n(s)$ and $G(s)$ curves at the respective temperatures. The decrease of the temperature shifts the position of $s_L$ towards higher $s$, and this shift is exactly the same as the shift of the maxima in $n(s)$ and $G(s)$. Thus, it appears that in this sample it is the crossover from the chain region to lattice region at $s_L$ which produces the maximum enhancement of pinning by RU domains. The enhancement is reduced at $s$ smaller than $s_L$ because the RU domains become more distant and the total area of the RU domains decreases. The enhancement is also precipitously reduced at $s$ larger than $s_L$ because domains in the disordered lattice become less distant and multiply interconnected. While the first factor leads to the increase of $v$-$v$ interactions between vortices pinned by neighboring domains, the second allows for easier vortex flow, and both effects combined produce strong decrease of the $n$ and $G$.

Figure 8(a) shows that the situation is different in case of the Pt3 sample because $s_L$ is larger, and large $\Delta a_{Lg}$ produces broad transition to vortex lattice region, as illustrated by broad hatched area. This suggests that while at large $s$ the vortex lattice is formed, it is most likely confined to spatially limited areas of the sample. This is, in fact, what could be expected in the presence of strongly disordered RU domain pattern.

It is possible that the transition from the vortex chains to the vortex lattice may explain the different $T$ dependencies of the magnetic pinning observed in small- and large-$s$ regions. In the chain region, large distances between RU domains limit $v$-$v$ interactions between neighboring domains. Therefore, the behavior of vortices is governed mainly by the interplay of $v$-$d$ interactions and $v$-$v$ interaction inside the chain structure. On the other hand, in the lattice region, while $v$-$d$ interactions provide the pinning centers, these are $v$-$v$ correlations in the lattice which are likely a dominating factor affecting the vortex dynamics. Intuitively, it may be expected that the $T$ dependence (which ultimately results from the $T$ dependence of $\Lambda$) should be weaker in case of chain structure. However, the detail theoretical evaluation of both situations is needed, and this is beyond the scope of this paper.

Finally, we would like to comment on the possible explanation of the different speeds of the flux expulsion from the two SFBs, as evidenced by the behavior of $F(s)$ (Fig. 3). This speed is comparable in the limit of small $s_+ < 0.1$ (i.e., essentially in the vortex chain region), but drops by half in the Pt14 sample when the region of vortex lattice is approached. At first glance, it seems counterintuitive that in the presence of easy vortex flow and small vortex confinement in the Pt14 sample the flux is expelled more slowly than in the case of Pt3, in which the vortices are very effectively trapped by RU domains of diverse widths, and vortex flow is impeded. However, we believe that the origin of this difference may be traced precisely to larger disorder in the domain pattern of the Pt3 sample. Namely, large disorder in the domain pattern induces very nonuniform pinning force density across the sample. In the areas of lower density of pinning force the flux unpins first. Because of $v$-$v$ correlations, any such unpinning event is likely to trigger the unpinning of vortices also in the neighboring areas with larger density of pinning force, quite possibly by a mechanism similar to thermomagnetic instabilities leading to the flux avalanches

in thin superconducting films [58,59]. This results in a large flux jump and a very rapid expulsion of flux. On the other hand, in the Pt14 sample, the density of pinning force is much more uniform, particularly when Pt14 enters the range of vortex lattice. While small flux jumps still occur during flux expulsion, their spatial extent is more limited, and the flux exit proceeds more smoothly and slowly.

## V. SUMMARY AND CONCLUSIONS

We have studied the influence of magnetic domain landscape on the flux dynamics in two SFBs with the F layers built from Co/Pt multilayers with perpendicular magnetic anisotropy. The thicknesses of platinum layers in the two SFBs are different, which results in very different geometry of the residual magnetic domains, which are reversibly defined by the partial magnetic reversal process. The domain patterns may be tuned, from a maze of wide multiply interconnected domains, to narrow well-isolated domains. The patterns in two SFBs differ by the dispersion of the domain widths. In addition, the narrow domains in one SFB are short, while in the other they are elongated, reaching across the sample.

Using a line of miniature Hall sensors, we observe that these differences in magnetic domain landscape affect profoundly the vortex dynamics in the SFBs. The differences appear in the flux confinement at the sample edge, the enhancement of flux pinning measured across the sample, and related to it, critical current density, and in the dynamics of flux expulsion. The largest flux confinement at the sample edge is observed in the presence of narrow, short, and well-isolated domains, while elongated domains induce much smaller confinement and guide vortices inside the sample for easy vortex entry. As a result, the pattern of narrow, elongated domains produces the largest enhancement of flux pinning and the critical current density (up to a factor of more than 7), while short domains limit the magnitude of the enhancement. However, when domains become wide, the disorder in the domain widths becomes beneficial for larger enhancement of pinning, while more uniform distribution of domain widths results in a precipitous drop of the enhancement. The flux expulsion is much more rapid in the presence of disordered domain landscape, and it is smooth and slow when the disorder is small. Finally, we observe that with the decrease of the temperature, the magnetic pinning increases. In the region of narrow domains, the increase is weaker than that of the nonmagnetic pinning, but in the wide domain range the $T$-induced changes of magnetic and nonmagnetic pinning are comparable.

We discuss these properties in terms of possible vortex arrangements above the magnetic domains. Two possible arrangements are shown to be compatible with the measured vortex density. The vortex chains are most likely formed above narrow, distant domains, while the wide domains allow for the formation of a distorted triangular vortex lattice. These considerations suggest that the largest enhancement of pinning appears at the transition from the chain to lattice region in the SFB with elongated domains of uniform width, when both the vortices inside the chains, and vortices pinned by neighboring domains, are simultaneously correlated.

## ACKNOWLEDGMENTS

This work was supported by Polish National Science Centre Grants No. 2011/01/B/ST3/00462 and No. 2014/15/B/ST3/03889, by the French-Polish Bilateral Program PICS 2012, by NSF Grant No. DMR12-622253, and by the European Union within the European Regional Development Fund, through the Innovative Economy Grant No. POIG.01.01.02-00-108/09.

[1] I. F. Lyuksyutov and V. L. Pokrovsky, Adv. Phys. **54**, 67 (2004).
[2] A. A. Golubov, M. Yu. Kupriyanov, and E. Il'ichev, Rev. Mod. Phys. **76**, 411 (2004).
[3] A. I. Buzdin, Rev. Mod. Phys. **77**, 935 (2005).
[4] F. S. Bergeret, A. F. Volkov, and K. B. Efetov, Rev. Mod. Phys. **77**, 1321 (2005).
[5] K. B. Efetov, I. A. Garifullin, A. F. Volkov, and K. Westerholt, *Magnetic Heterostructures* (Springer-Verlag, Berlin, Heidelberg, 2008).
[6] A. Yu. Aladyshkin, A. V. Silhanek, W. Gillijns, and V. V. Moshchalkov, Supercond. Sci. Technol. **22**, 053001 (2009).
[7] A. Y. Aladyshkin, A. I. Buzdin, A. A. Fraerman, A. S. Melnikov, D. A. Ryzhov, and A. V. Sokolov, Phys. Rev. B **68**, 184508 (2003).
[8] A. Yu. Aladyshkin and V. V. Moshchalkov, Phys. Rev. B **74**, 064503 (2006).
[9] Z. Yang, M. Lange, A. Volodin, R. Szymczak, and V. V. Moshchalkov, Nat. Mater. **3**, 793 (2004).
[10] W. Gillijns, A. Yu. Aladyshkin, M. Lange, M. J. Van Bael, and V. V. Moshchalkov, Phys. Rev. Lett. **95**, 227003 (2005).
[11] W. Gillijns, A. Yu. Aladyshkin, A. V. Silhanek, and V. V. Moshchalkov, Phys. Rev. B **76**, 060503(R) (2007).
[12] L. Y. Zhu, M. Z. Cieplak, and C. L. Chien, Phys. Rev. B **82**, 060503(R) (2010).
[13] M. Velez, J. I. Martín, J. E. Villegas, A. Hoffmann, E. M. González, J. L. Vicent, and I. K. Schuller, J. Magn. Magn. Mater. **320**, 2547 (2008).
[14] L. N. Bulaevskii, E. M. Chudnovsky, and M. P. Maley, Appl. Phys. Lett. **76**, 2594 (2000).
[15] Yu. I. Bezpyatykh, W. Wasilevski, M. Gajdek, I. P. Nikitin, and S. A. Nikitov, Phys. Solid State **43**, 1827 (2001).
[16] M. V. Milosevic, S. V. Yampolskii, and F. M. Peeters, Phys. Rev. B **66**, 174519 (2002).
[17] S. Erdin, I. F. Lyuksyutov, V. L. Pokrovsky, and V. M. Vinokur, Phys. Rev. Lett. **88**, 017001 (2001).
[18] E. B. Sonin, Phys. Rev. B **66**, 136501 (2002).
[19] R. Laiho, E. Lahderanta, E. B. Sonin, and K. B. Traito, Phys. Rev. B **67**, 144522 (2003).
[20] M. A. Kayali and V. L. Pokrovsky, Phys. Rev. B **69**, 132501 (2004).

[21] S. Erdin, Phys. Rev. B **73**, 224506 (2006).

[22] J. I. Martin, M. Vélez, J. Nogués, and I. K. Schuller, Phys. Rev. Lett. **79**, 1929 (1997).

[23] J. I. Martin, M. Velez, A. Hoffmann, I. K. Schuller, and J. L. Vicent, Phys. Rev. Lett. **83**, 1022 (1999).

[24] D. J. Morgan and J. B. Ketterson, Phys. Rev. Lett. **80**, 3614 (1998).

[25] M. J. Van Bael, K. Temst, V. V. Moshchalkov, and Y. Bruynseraede, Phys. Rev. B **59**, 14674 (1999).

[26] S. Kolesnik, V. Vlasko-Vlasov, U. Welp, G. W. Crabtree, T. Piotrowski, J. Wrobel, A. Klimov, P. Przyslupski, T. Skoskiewicz, and B. Dabrowski, Physica C (Amsterdam) **341-348**, 1093 (2000).

[27] M. Velez, D. Jaque, J. I. Martin, M. I. Montero, I. K. Schuller, and J. L. Vicent, Phys. Rev. B **65**, 104511 (2002).

[28] J. E. Villegas, S. Savel'ev, F. Nori, E. M. Gonzalez, J. V. Anguita, R. Garcia, and J. L. Vicent, Science **302**, 1188 (2003).

[29] J. E. Villegas, M. I. Montero, C.-P. Li, and I. K. Schuller, Phys. Rev. Lett. **97**, 027002 (2006).

[30] M. Kemmler, D. Bothner, K. Ilin, M. Siegel, R. Kleiner, and D. Koelle, Phys. Rev. B **79**, 184509 (2009).

[31] C. Reichhardt and C. J. Olson Reichhardt, Phys. Rev. B **76**, 094512 (2007).

[32] F. Laviano, L. Gozzelino, E. Mezzetti, P. Przyslupski, A. Tsarev, and A. Wisniewski, Appl. Phys. Lett. **86**, 152501 (2005).

[33] V. Vlasko-Vlasov, U. Welp, G. Karapetrov, V. Novosad, D. Rosenmann, M. Iavarone, A. Belkin, and W.-K. Kwok, Phys. Rev. B **77**, 134518 (2008).

[34] A. Garcia-Santiago, F. Sanchez, M. Varela, and J. Tejada, Appl. Phys. Lett. **77**, 2900 (2000).

[35] X. X. Zhang, G. H. Wen, R. K. Zheng, G. C. Xiong, and G. J. Lian, Europhys. Lett. **56**, 119 (2001).

[36] D. B. Jan, J. Y. Coulter, M. E. Hawley, L. N. Bulaevskii, M. P. Maley, Q. X. Jia, B. B. Maranville, F. Hellman, and X. Q. Pan, Appl. Phys. Lett. **82**, 778 (2003).

[37] M. Lange, M. J. Van Bael, V. V. Moshchalkov, and Y. Bruynseraede, Appl. Phys. Lett. **81**, 322 (2002).

[38] M. Z. Cieplak, X. M. Cheng, C. L. Chien, and Hai Sang, J. Appl. Phys. **97**, 026105 (2005).

[39] M. Z. Cieplak, Z. Adamus, A. Abal'oshev, I. Abal'osheva, M. Berkowski, X. M. Cheng, Hai Sang, and C. L. Chien, Phys. Status Solidi C **2**, 1650 (2005).

[40] M. Feigenson, L. Klein, M. Karpovski, J. W. Reiner, and M. R. Beasley, J. Appl. Phys. **97**, 10J120 (2005).

[41] M. Z. Cieplak, L. Y. Zhu, Z. Adamus, M. Kończykowski, and C. L. Chien, Phys. Rev. B **84**, 020514(R) (2011).

[42] G. Karapetrov, M. V. Milošević, M. Iavarone, J. Fedor, A. Belkin, V. Novosad, and F. M. Peeters, Phys. Rev. B **80**, 180506(R) (2009).

[43] M. Iavarone, A. Scarfato, F. Bobba, M. Longobardi, G. Karapetrov, V. Novosad, V. Yefremenko, F. Giubileo, and A. M. Cucolo, Phys. Rev. B **84**, 024506 (2011).

[44] M. Z. Cieplak, Z. Adamus, M. Kończykowski, L. Y. Zhu, X. M. Cheng, and C. L. Chien, Phys. Rev. B **87**, 014519 (2013).

[45] J. W. Knepper and F. Y. Yang, Phys. Rev. B **71**, 224403 (2005).

[46] To calculate $s$ from magnetization measurement, we first subtract the background $M(H)$, visible at the top and bottom parts of the hysteresis loop in Fig. 1(b), which originates from paramagnetic parts of the sample and spurious signals from the sample holder. This background is completely absent in $R_H(H)$ dependence.

[47] J. E. Davies, O. Hellwig, E. E. Fullerton, G. Denbeaux, J. B. Kortright, and K. Liu, Phys. Rev. B **70**, 224434 (2004).

[48] G. Bochi, H. J. Hug, D. I. Paul, B. Stiefel, A. Moser, I. Parashikov, H.-J. Güntherodt, and R. C. O'Handley, Phys. Rev. Lett. **75**, 1839 (1995).

[49] V. Baltz, A. Marty, B. Rodmacq, and B. Dieny, Phys. Rev. B **75**, 014406 (2007).

[50] M. Tinkham, *Introduction to Superconductivity* (Dover, New York, 2004).

[51] G. M. Maksimova, R. M. Ainbinder, and D. Y. Vodolazov, Phys. Rev. B **78**, 224505 (2008).

[52] C. P. Bean, Phys. Rev. Lett. **8**, 250 (1962); Rev. Mod. Phys. **36**, 31 (1964).

[53] W. T. Norris, J. Phys. D: Appl. Phys. **3**, 489 (1970); Y. Yang, T. Hughes, C. Beduz, D. M. Spiller, R. G. Scurlock, and W. T. Norris, Physica C (Amsterdam) **256**, 378 (1996).

[54] E. H. Brandt, M. Indenbom, and A. Forkl, Europhys. Lett. **22**, 735 (1993); E. H. Brandt and M. Indenbom, Phys. Rev. B **48**, 12893 (1993); E. H. Brandt, *ibid.* **49**, 9024 (1994); Phys. Rev. Lett. **71**, 2821 (1993).

[55] E. Zeldov, J. R. Clem, M. McElfresh, and M. Darwin, Phys. Rev. B **49**, 9802 (1994).

[56] E. H. Brandt, Phys. Rev. B **54**, 4246 (1996).

[57] A. V. Silhanek, J. Gutierrez, R. B. G. Kramer, G. W. Ataklti, J. Van de Vondel, V. V. Moshchalkov, and A. Sanchez, Phys. Rev. B **83**, 024509 (2011).

[58] E. Altshuler, Rev. Mod. Phys. **76**, 471 (2004).

[59] D. V. Denisov, D. V. Shantsev, Y. M. Galperin, E.-M. Choi, H. S. Lee, S. I. Lee, A. V. Bobyl, P. E. Goa, A. A. F. Olsen, and T. H. Johansen, Phys. Rev. Lett. **97**, 077002 (2006).